Int J Appl Earth Obs Geoinformation 63 (2017) 234–243

Contents lists available at ScienceDirect

Int J Appl Earth Obs Geoinformation

journal homepage: www.elsevier.com/locate/jag

Research Paper

Evaluating MODIS snow products for modelling snowmelt runoff: Case study of the Rio Grande headwaters

Caitriana Steele[a,b,*], John Dialesandro[c], Darren James[a], Emile Elias[a], Albert Rango[a], Max Bleiweiss[b]

[a] USDA-ARS Jornada Experimental Range, Las Cruces, NM, USA
[b] Department of Plant and Environmental Sciences, New Mexico State University, Las Cruces, NM, USA
[c] Department of Geography, University of California, Davis, CA, USA

ARTICLE INFO

Keywords:
MODIS snow products
MOD10A1
MODSCAG
Snow covered area
Snowmelt Runoff Model

ABSTRACT

Snow-covered area (SCA) is a key variable in the Snowmelt-Runoff Model (SRM) and in other models for simulating discharge from snowmelt. Landsat Thematic Mapper (TM), Enhanced Thematic Mapper (ETM +) or Operational Land Imager (OLI) provide remotely sensed data at an appropriate spatial resolution for mapping SCA in small headwater basins, but the temporal resolution of the data is low and may not always provide sufficient cloud-free dates. The coarser spatial resolution Moderate Resolution Imaging Spectroradiometer (MODIS) offers better temporal resolution and in cloudy years, MODIS data offer the best alternative for mapping snow cover when finer spatial resolution data are unavailable. However, MODIS' coarse spatial resolution (500 m) can obscure fine spatial patterning in snow cover and some MODIS products are not sensitive to end-of-season snow cover. In this study, we aimed to test MODIS snow products for use in simulating snowmelt runoff from smaller headwater basins by a) comparing maps of TM and MODIS-based SCA and b) determining how SRM streamflow simulations are changed by the different estimates of seasonal snow depletion. We compared gridded MODIS snow products (Collection 5 MOD10A1 fractional and binary SCA; SCA derived from Collection 6 MOD10A1 Normalised Difference Snow Index (NDSI) Snow Cover), and the MODIS Snow Covered-Area and Grain size retrieval (MODSCAG) canopy-corrected fractional SCA (SCA_{MG}), with reference SCA maps (SCA_{REF}) generated from binary classification of TM imagery. SCA_{MG} showed strong agreement with SCA_{REF}; excluding true negatives (where both methods agreed no snow was present) the median percent difference between SCA_{REF} and SCA_{MG} ranged between −2.4% and 4.7%. We simulated runoff for each of the four study years using SRM populated with and calibrated for snow depletion curves derived from SCA_{REF}. We then substituted in each of the MODIS-derived depletion curves. With efficiency coefficients ranging between 0.73 and 0.93, SRM simulation results from the SCA_{MG} runs yielded the best results of all the MODIS products and only slightly underestimated discharge volume (between 7 and 11% of measured annual discharge). SRM simulations that used SCA derived from Collection 6 NDSI Snow Cover also yielded promising results, with efficiency coefficients ranging between 0.73 and 0.91.

In conclusion, we recommend that when simulating snowmelt runoff from small basins (< 4000 km^2) with SRM, we recommend that users select either canopy-corrected MODSCAG or create their own site-specific products from the Collection 6 MOD10A1 NDSI.

1. Introduction

In the mountainous regions of the western United States, springtime snowmelt dominates the hydrographs of most major river systems, with spring and summer contributions representing 50–80% of the total annual discharge (Stewart et al., 2004). Of increasing concern are the potential effects of climate change on annual snowpack and snowmelt runoff. The magnitude of the decline of the annual snowpack over the latter part of the 20th century has no analogy in the climate record from the last millennium (Pederson et al., 2011). Forming an understanding of how climate change will affect streamflow is essential for planning water resources. One path to developing this knowledge is through models that simulate hydrological discharge in snow-fed systems.

Snowmelt models are usually classified as either temperature index

* Corresponding author.
E-mail address: caiti@nmsu.edu (C. Steele).

http://dx.doi.org/10.1016/j.jag.2017.08.007
Received 25 February 2015; Received in revised form 26 July 2017; Accepted 10 August 2017

(TI) or energy balance (EB) models. The TI approach treats temperature as the primary control on snowmelt, and because of this, data requirements are modest. Air temperature is assumed to act as a proxy for longwave atmospheric radiation, absorbed global radiation, and sensible heat flux, all of which contribute to snowmelt (Ohmura, 2001). In the TI model, the rate of ablation is calculated from the sum of positive air temperatures in a given time interval (Hock, 2003). The degree-day factor relates daily snowmelt rates to air temperature and it is this parameter that is modified to maximise agreement between air temperature and snowmelt. Other parameters accounting for loss through processes such as infiltration or sublimation may also be tweaked to optimize model performance. Many studies have demonstrated the successful application of TI models for modelling snowmelt (e.g., Lee et al., 2005; Tekeli et al., 2005; Li and Williams, 2008) and for simulating how streamflow will change under a warming climate (Elias et al., 2015). TI models are also widely used in operational settings (e.g., SNOW-17; Anderson, 1976). However, TI models perform poorly in complex situations where temperature is not a good proxy for energy exchange processes that contribute to snowmelt (Garen and Marks, 2005).

EB models are process-based models of snowmelt that represent energy fluxes between soil, snow and atmosphere. They depend on the physical laws of radiative, sensible, latent and adjective heat exchanges, and as such they do not require calibration (Marks et al., 1999). EB models often have intensive data requirements but advocates argue that the physical basis of these models means that they more accurately represent spatial patterns of melt (Kumar et al., 2013). A principal challenge with using the EB approach is simply that the data may not be available, particularly in more isolated mountain areas (Day, 2009).

There are examples of both types of model that require remotely-sensed snow covered area (SCA) (e.g., Martinec et al., 2008; Andreadis and Lettenmaier, 2006; Homan et al., 2011). Usually, the input takes the form of a depletion curve generated for the study basin or elevation zones within a study basin. For example, the Snowmelt Runoff Model (SRM) requires daily SCA estimates per ~500 m elevation zone (Martinec et al., 2008). Over the last 20+ years, there has been an increasing availability of ready-made snow products of varying spatial resolutions, from sensors such as the Advanced Very High Resolution Radiometer (AVHRR), Special Sensor Microwave/Imager (SSMI), Advanced Microwave Scanning Radiometer − Earth Observing System (AMSR-E), and the Moderate Resolution Imaging Spectroradiometer (MODIS) instruments. Of these, the MODIS snow products (MOD10) developed by Hall et al. (1995) and distributed by the National Snow and Ice Data Center (NSIDC) are probably the most widely-used for hydrological modelling; they are of moderate spatial resolution (500 m) and require minimal processing to provide SCA estimates. MOD10 binary snow products have been successfully applied by other studies requiring remotely sensed snow cover estimates to drive SRM (Lee et al., 2005; Tekeli et al., 2005; Li and Williams, 2008; Georgievsky, 2009; Immerzeel et al., 2009; Panday et al., 2013). To date, we have not found other authors who have tested fractional products in SRM. It is noteworthy that these standard MOD10 products are generated from global algorithms, and as such are not optimized to any particular region. However, the new Collection 6 (C6) MOD10 product supplies the Normalized Difference Snow Index (NDSI) rather than snow cover. This means that users have the option to modify the NDSI using the global empirical model (Riggs et al., 2016) or they can develop their own region-specific model.

An alternative snow product is available from the Snow Data System hosted by the National Aeronautics and Space Administration (NASA) Jet Propulsion Laboratory. The MODIS Snow Covered-Area and Grain size retrieval (MODSCAG) algorithm is based on multiple end-member spectral mixture analysis with endmembers derived from snow, vegetation, rock, soil and lake ice (Painter et al., 2009). The operational algorithm uses the same end-members for all snow-covered regions and calculates the relative contribution of each end-member component using sets of simultaneous linear equations.

Our research objective here is to assess the applicability of MODIS snow products for deriving SCA estimates for SRM, specifically over a small headwater basin. Some researchers report success with snow cover algorithms based on spectral mixture modelling (Shreve et al., 2009; Rittger et al., 2013). Other researchers have successfully applied NDSI-based techniques, reporting accuracies ranging from 88 to 93% (Hall and Riggs, 2007; Riggs and Hall, 2015). Like any model, the value of SRM to provide meaningful short- or long-term predictions of streamflow, depends greatly on the quality of the original input data. Under- or over-estimation of SCA inputs in a TI model such as SRM will directly impact model calibration. Then, if model parameters are incorrectly adjusted to account for SCA errors, then this is carried forward into climate change runs yielding erroneous results of future projections of streamflow. We tested MOD10 gridded snow cover products (MOD10A1) and MODSCAG canopy-corrected snow cover against reference data derived from Landsat Thematic Mapper (TM) imagery (spatial resolution 30 m). We also compare the output of SRM simulations using the different SCA estimates from the MODIS and TM snow cover products.

2. Methods

2.1. Study basin

For this case study we use the Upper Rio Grande (URG) headwater basin above Del Norte gauge, Colorado (hereafter referred to as 'Del Norte') because it is the largest and most productive sub-basin in the URG; additionally, we have experience in modelling this basin dating back to some of the earliest SRM work (Martinec et al., 1983). The Del Norte sub-basin is located in the San Juan Mountains of south-central Colorado (Fig. 1). The size of the sub-basin as delimited for this study is 3416 km^2. Elevation ranges from 2436 to 4222 m. We divided Del Norte into 3 elevation zones for SRM simulations (Fig. 1). Zone 3 (3353–4222 m) falls largely above the treeline and is dominated by alpine tundra. Dense subalpine coniferous forests comprise much of the vegetation in Zone 2 (2926–3352 m) and are also present in Zone 1 and Zone 3. Zone 1 (2436–2925 m) has large expanses of meadow and where there is evergreen forest canopy cover, it often has a more open canopy than that of the subalpine coniferous forests in Zone 2. Stands of deciduous trees, riparian woodlands and meadows are also represented in all elevation zones. Annual snowpack accumulates throughout the winter months, melting in spring to yield the characteristic snowmelt hydrograph. About 75% of total annual streamflow volume passes through the gauge between April 1st and July 31st, with peak streamflow usually occurring in late May. In a very dry year, the Del Norte basin produces about 97 million cubic meters between April and July; in a productive year, the Del Norte basin can yield well over 700 million cubic meters between April and July. Snow persistence through the spring snowmelt season depends on the initial conditions of the snowpack, and exposure to rising temperatures and wind. Wind-exposed, unvegetated ridges at higher elevations usually lose snow cover before the onset of snowmelt; by contrast, at mid- to upper elevations, shaded snowpack in gullies and under forest canopies may persist in patches through to late June. There are several small reservoirs located in the Del Norte sub-basin which are used for storing water for agriculture in the nearby San Luis Valley. There are also minor diversions between these reservoirs. However, discharge measured at the Rio Grande at Del Norte Stream Gage is predominantly natural flow.

2.2. Remote sensing data preparation for SRM

2.2.1. Creating reference snow maps from landsat TM imagery

We were interested in comparing the MODIS coarse spatial resolution products against a finer spatial resolution reference SCA product. Our only option for creating this reference product was to use

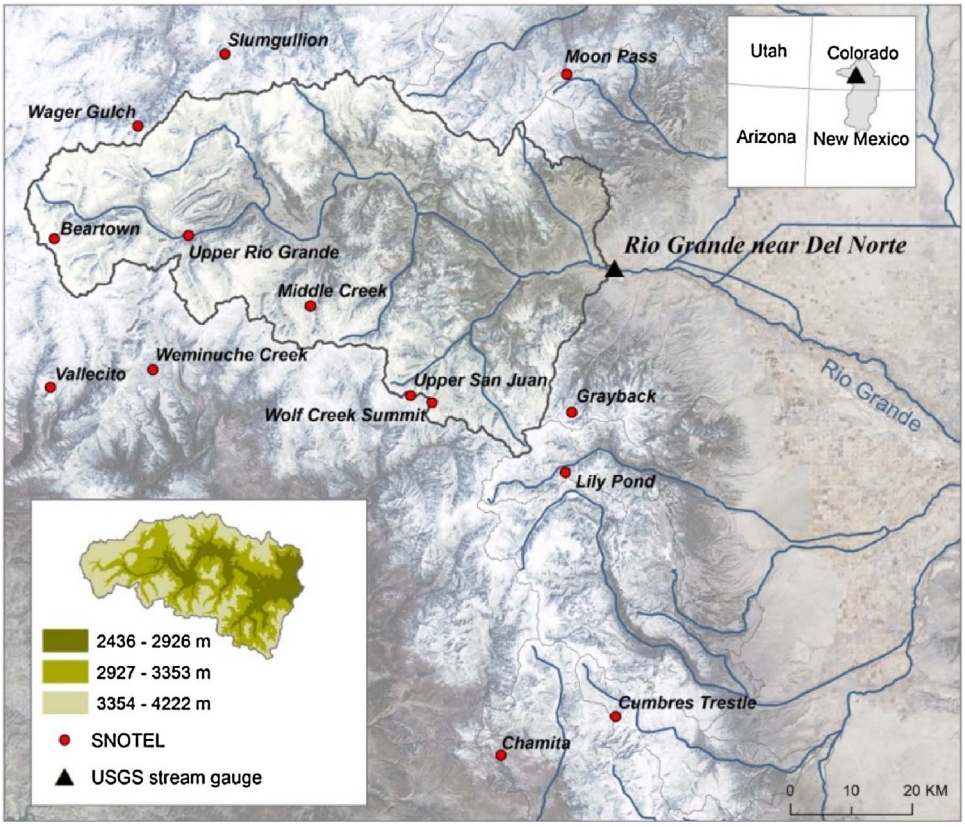

Fig. 1. Rio Grande headwaters in southern Colorado. Lower map insert shows elevation zones used for SRM model input.

coincident imagery from Landsat sensors, which with a pixel size of 30 m m, have a much finer spatial resolution than MODIS sensors. We selected 2001, 2008, 2010 and 2011 for analysis because each of these years had at least five cloud-free acquisitions of Landsat Thematic Mapper (TM) imagery for the months of March − July. Enhanced Thematic Mapper Plus (ETM +) imagery was also available for 2001. We downloaded Surface Reflectance Climate Data Record (CDR) atmospherically-corrected data from EarthExplorer (USGS, 2016a) for 22 dates across the four test years.

To classify pixels as snow-covered or snow-free, we used the binary mapping algorithm that was originally proposed by Riggs et al. (1994) for use with TM and MODIS data, and later modified by Klein et al. (1998). This algorithm also forms the basis for the MODIS binary snow cover product (Riggs et al., 2006). It uses the NDSI, the normalized difference vegetation index (NDVI) and reflectance in green and near-infrared wavebands. For TM and ETM+ data, the NDSI is formulated as:

$$NDSI = \rho_{0.56} - \rho_{1.65} / \rho_{0.56} + \rho_{1.65} \quad (1)$$

And the NDVI is formulated as

$$NDVI = \rho_{0.66} - \rho_{0.83} / \rho_{0.66} + \rho_{0.83} \quad (2)$$

Where $\rho_{0.56}$ is reflectance in band 2 (green wavelengths), $\rho_{1.65}$ is reflectance in band 5 (shortwave infrared (SWIR) wavelengths), $\rho_{0.66}$ is reflectance in band 3 (red wavelengths) and $\rho_{0.83}$ is reflectance in band 4 (NIR wavelengths). A pixel is classified as snow if NDSI ≥ 0.4, band 2 reflectance > 0.11 and NIR reflectance > 0.10. We selected the NDSI ≥ 0.4 threshold based on findings reported by Dozier (1989) and Riggs et al. (1994). We assessed the accuracy of the resulting SCA reference maps and report these results in Section 3.1.

This ruleset does not account for heavily vegetated areas where tree cover may reduce NDSI values to values below the 0.4 threshold. To account for this, snow field vectors plotted in NDSI-NDVI feature space are used as additional criteria to map snow in vegetated areas (Klein et al., 1998). For the research presented here, the algorithm was scripted in R and is available from the authors.

To ascertain the accuracy of the TM binary product, we used random sampling to identify 150 testing pixels per elevation zone: 450 testing pixels in total per data set. Of this sample 75 pixels were randomly selected in late season, high elevation snowpack to ensure adequate sampling of the snow class as it becomes more limited in extent. Testing pixels were assigned the label *snow* or *no snow* depending on visually-interpreted values in bands 5, 4 and 3 and with reference to landscape position, vegetation cover interpreted from fine spatial resolution imagery (ESRI, 2016), elevation, and proximity to visible snowpack.

2.2.2. MODIS data

MOD10A1 Collection 5 (C5) and Collection 6 (C6) gridded daily snow cover products (Hall et al., 2006; Hall and Riggs, 2016) were downloaded from NASA's Reverb metadata and service discovery tool (EOSDIS, 2009) for dates between February and July for 2001, 2008, 2010 and 2011. C6 differs from C5 in that the C5 binary product (SCA_{BN-C5}) and the C5 fractional product (SCA_{F-C5}) are no longer included. Both have been replaced with "NDSI Snow Cover" (Riggs et al., 2016). An advantage of the C6 product is that it does not use the surface temperature screen used in C5 products, which caused missed snow cover in late spring and early summer (Riggs et al., 2016). Additionally, methods for reducing snow cover errors of commission and omission have been revised in C6 (Riggs et al., 2016).

To generate SCA from NDSI Snow Cover, users can apply the globally-determined linear model (3) supplied in Riggs et al. (2016) or develop a site specific relationship between NDSI and snow cover using a methodology similar to Salomonsson and Appel (2004). Using (3) would create a product similar to SCA_{F-C5}. For this study, we analysed the relationship between C6 NDSI Snow Cover and percent snow cover identified using TM and ETM imagery. The ten dates of good quality coincident imagery described in Section 2.2.3 provided the data for this

analysis. The resulting empirical relation is shown below in (4). Subscript 'URG' is used to indicate that Eq. (4) was developed for the Upper Rio Grande and is not globally applicable.

$$SCA_{F\text{-}C5} = -0.01 + 1.45(NDSI) \quad (3)$$

$$SCA_{F\text{-}C6\text{-}URG} = 7.017 + 1.24(NDSI) \quad (4)$$

The higher slope coefficient in (3) results in larger SCA estimates from higher NDSI values than for (4), whereas the higher intercept coefficient in (4) results in comparatively larger SCA estimates from lower NDSI values than for (3).

Canopy-corrected MODSCAG data were downloaded from the Snow Data System hosted by NASA's Jet Propulsion Laboratory (Painter et al., 2009). MODSCAG fractional SCA (f_{SCA}) estimates give viewable snow-covered area and do not account for sub-canopy snow. The canopy corrected product ($f_{SCA,adjusted}$) is calculated using the estimated fractional forest cover (f_{can}) in the following formula (Rittger et al., 2013):

$$f_{SCA,adjusted} = \frac{f_{SCA}}{1 - f_{can}} \quad (5)$$

(Note that to simplify abbreviations in this paper, we use "SCA_{MG}" for $f_{SCA,adjusted}$).

We used only Terra MODIS data for this study because Terra's daytime overpass is close in time to that of the Landsat satellites. We also excluded any data acquired with a sensor zenith angle greater than 30°. Other research has shown that large sensor zenith angles may result in underestimation of fractional snow cover; as sensor zenith angle increases, forest canopies progressively obscure more of the ground surface (Xin et al., 2012). Invalid pixels and cloud cover were assessed by elevation zone. Zonal SCA estimates were excluded from further analysis if more than 10% of zone area was affected by invalid pixels and cloud cover combined, or if no snow was detected. After screening, 69 dates of MODIS data were selected for modelling annual snow cover depletion.

2.2.3. Comparing snow cover estimates

We compared the four MODIS-based snow cover products with the reference TM binary product (SCA_{REF}), selecting comparison dates that were within 0–3 days of image acquisition. Because we excluded MODIS data with sensor zenith angles greater than 30°, direct comparison between MODIS and TM was optimal for 10 of the 22 TM and ETM+ datasets. If dates were not coincident, we selected the best available MODIS imagery that predated TM imagery.

To compare the $SCA_{BN\text{-}C5}$, $SCA_{F\text{-}C5}$, $SCA_{F\text{-}C6\text{-}URG}$, and SCA_{MG} datasets with SCA_{REF}, we first calculated the area of snow in MODIS and TM pixels. Rather than resampling the MODIS and TM data to a common resolution, we extracted the area of snow from each dataset using a vector-based sampling grid where each cell was 1500 by 1500 m in size. This vector grid was created using the Fishnet tool in ArcGIS (ESRI, 2015). We then calculated the percent difference between TM-based and MODIS-based snow area estimates for each sampling cell.

2.3. Snowmelt Runoff Model

SRM is a deterministic, semi-distributed, daily time-step, TI model: it has been used successfully to simulate runoff snowmelt in basins ranging in size from 0.76 km^2 to 917,444 km^2 (Martinec et al., 2008). Originally developed to run with temperature and precipitation inputs, remotely sensed SCA estimates were introduced to the model by Rango and Martinec (1979). SRM is formulated as

$$Q_{n+1} = [c_{Sn}\cdot\alpha_n(T_n + \Delta T_n)S_n + c_{Rn}P_n]\cdot(A\cdot 10{,}000)/86{,}400\cdot(1 - k_{n+1}) + Q_n k_{n+1} \quad (6)$$

Average daily discharge (Q: $m^3\,s^{-1}$) on day n+1 is the sum of snowmelt, precipitation and discharge on the preceding day (n). The snowmelt function calculates snowmelt as the product of the fraction of snow covered area (S), the degree day factor (α: cm °C^{-1} d^{-1}), zonal degree days ($T+\Delta T$: °C d) and the snowmelt runoff loss coefficient (c_S). Runoff from liquid precipitation is calculated as the product of measured precipitation (P: cm) and the rainfall runoff loss coefficient (c_R). Discharge decline in snowmelt- or precipitation-free periods is indicated by a basin-specific recession coefficient (k). The factor (A 10,000)/86,400 converts from cm km^{-2} d^{-1} to $m^3\,s^{-1}$ where A is basin area.

The snowmelt function within SRM relates increasing air temperature to declining SCA to give estimates of input from snowmelt to streamflow. This function requires daily estimates of the proportion of each elevation zone covered with snow, including sub-canopy snow cover. End-of-winter snowpack may have the same areal coverage from year to year but very different values for snow water equivalent (SWE). Higher SWE translates to slower reduction of SCA. Thus, together with temperature, the snow cover depletion variable controls how fast snowpack is melting within the model and how much water the snowpack is expected to deliver over the melt season.

2.3.1. Snow cover inputs for SRM

Daily remotely sensed estimates of SCA are available from sensors such as MODIS, but are often contaminated by cloud cover; or for wide field-of-view sensors, there may be issues associated with sensor zenith angle. For optimal model performance, snow cover data for SRM should be restricted to dates where there is minimal uncertainty introduced by non-ideal sensor viewing or atmosphere conditions. For each of the TM- and MODIS-derived snow maps, we calculated the proportion of SCA in each zone for best available dates. Because daily snow data are not usually available, it is necessary to estimate SCA for missing dates. To derive daily SCA estimates (conventional depletion curves: CDCs) for each elevation zone, we fitted sigmoidal, logistic or exponential decay curves to the available SCA values. After April 1st, images containing fresh snowfall must be excluded. This is because SRM uses precipitation data to add to the available snowpack. If transient snow is included in modelling CDCs, then the snow input is added twice leading to potential overestimation of snowmelt contributions to discharge.

2.3.2. SRM simulations

We populated SRM with temperature, precipitation and streamflow data for the 2001, 2008, 2010 and 2011 water years. Data were sourced from (i) the National Resources Conservation Service (NRCS) Snow Telemetry (SNOTEL) network (NRCS, 2016); (ii) the National Oceanic and Atmospheric Administration (NOAA) National Climatic Data Center Cooperative Observer Network (COOP: NOAA, 2016) and (iii) the United States Geological Survey (USGS) National Water Information System database (USGS, 2016b).

For each year, we calibrated SRM for CDCs derived from the TM binary product. We then ran SRM with each of the MODIS CDC datasets to determine how streamflow simulations were changed by the differing estimates of snow cover. Using this method, differences in model output are driven solely by differences in CDCs modelled from TM and MODIS data.

3. Results and discussion

3.1. Assessment of SCA_{REF} maps

Table 1 shows the results for user's (errors of commission) and producer's (errors of omission) accuracy of the snow class and overall accuracy for each SCA_{REF} map. Most accuracy values exceed 0.9. For 2001 and 2010, errors of omission are lowest during the early snowmelt period when snow cover is extensive. Towards the end of the season in these years, errors of omission increase markedly. On closer examination of the input data, this can be explained by NDSI values dropping just below 0.4 for areas clearly still snow-covered. Errors of commission

Table 1
Accuracy assessment of the TM reference product (SCA_{REF}).

Date	Snow		Overall	Date	Snow		Overall
	U	*P*			*U*	*P*	
12/02/2001	0.99	1.00	0.99	15/06/2008	0.89	0.95	0.97
01/04/2001	0.99	0.99	0.99	17/03/2010	0.99	0.97	0.96
17/04/2001	0.98	0.99	0.98	04/05/2010	0.90	0.89	0.90
25/04/2001	0.95	1.00	0.96	20/05/2010	0.88	0.99	0.96
11/05/2001	0.93	0.96	0.94	05/06/2010	0.91	0.85	0.96
12/06/2001	0.90	0.88	0.96	21/06/2010	0.80	0.27	0.97
06/07/2001	0.93	0.54	0.97	20/03/2011	0.91	0.92	0.90
27/03/2008	0.97	0.96	0.94	04/04/2011	0.92	0.90	0.91
12/04/2008	0.98	0.99	0.98	07/05/2011	0.96	0.94	0.96
28/04/2008	0.92	0.98	0.94	08/06/2011	0.92	0.99	0.98
30/05/2008	0.93	0.99	0.97	24/06/2011	0.94	0.99	0.99

are highest towards the end of the season in 2008 and 2010. It is logical that classification accuracy declines as the snow pack ages. The reflectance properties may change for several reasons, including snow pack becoming more discontinuous or discoloured from dust. Impurities in the snowpack reduce visible reflectance more than shortwave infrared reflectance (Dozier, 1989). If visible reflectance decreases without a decrease in the shortwave infrared, NDSI will also decrease even though there may be no change in snow covered area.

SCA_{REF} maps created from the TM binary product were also compared against snow pillow and snow course data from 13 SNOTEL stations within the vicinity of the study area (Fig. 1). Twenty-two dates of imagery yield 250 possible comparisons. Our analysis supplied a user's accuracy of 0.98, producer's accuracy of 0.86 and an overall accuracy of 0.90. More errors of omission occurred towards the end of the snowmelt season in late May and June. These results should be viewed with caution, however, because the precision of the SNOTEL coordinates is not reported with the data.

3.2. Comparison of MODIS snow cover estimates with SCA_{REF}

Fig. 2 summarises the differences between SCA_{REF} and SCA estimated by each of the MODIS products. To simplify comparison, we calculated the percent difference between TM- and MODIS-based SCA. A 100% difference represents an area of 2.25 km^2 (the area of the 1500 m by 1500 m sampling units). We found some skewed frequency distributions of MODIS and TM differences, so rather than use statistics that assume normal distribution, we used the five number summary illustrated with box-and-whisker plots. We omitted "true negatives" where both methods agreed that no snow was present. The box represents the interquartile range (IQR), or the middle 50% of the data. The lower box boundary is the line is defined by the first quartile (Q1) and the upper box boundary is defined by the third quartile (Q3). Whiskers are calculated from 1.5IQR (Tukey, 1977) and represent 99.3% of the data. Outliers are those values that lie below or above 1.5IQR. Best agreements between products are indicated by median values close to zero, narrow boxes and short whiskers. In most cases, whiskers extend into positive and negative values meaning that on an individual date, a MODIS product can both under- and over-estimate SCA compared to SCA_{REF}. The position of the IQR on the x-axis is also relevant. We subtracted MODIS estimates from TM estimates, so a greater proportion of positive values show MODIS product underestimation compared to the TM binary product and a greater proportion of negative values show overestimation.

Of all the MODIS products, SCA_{MG} estimates are closest to SCA_{REF} for most of the snowmelt season. Overall, median values for the difference between SCA_{MG} and SCA_{REF}, are positioned much closer to 0% (ranging between −2.4% and 4.7%), the IQR is narrower than for the MOD10A1 C5 and C6 products, and it extends in approximately equal amounts into positive and negative values. Q1 ranges between −13% and 0.09%; Q3 ranges between 0 and 15.2%. Of the MOD10A1 products, $SCA_{BN\text{-}C5}$ tends to perform better than $SCA_{F\text{-}C5}$ or $SCA_{F\text{-}C6\text{-}URG}$ during the early snowmelt season (March, April, May). Early season median values for the difference between SCA_{REF} and $SCA_{F\text{-}C5}$ range between 0.02% and 10.5%, Q1 ranges between −1.86% and 0.76%, and Q3 ranges between 2.75% to 30.27%. These results show that the C5 binary product will be more likely to overestimate snow cover on some occasions and underestimate snow cover on others; underestimation is a known problem at the end of the snowmelt season, but

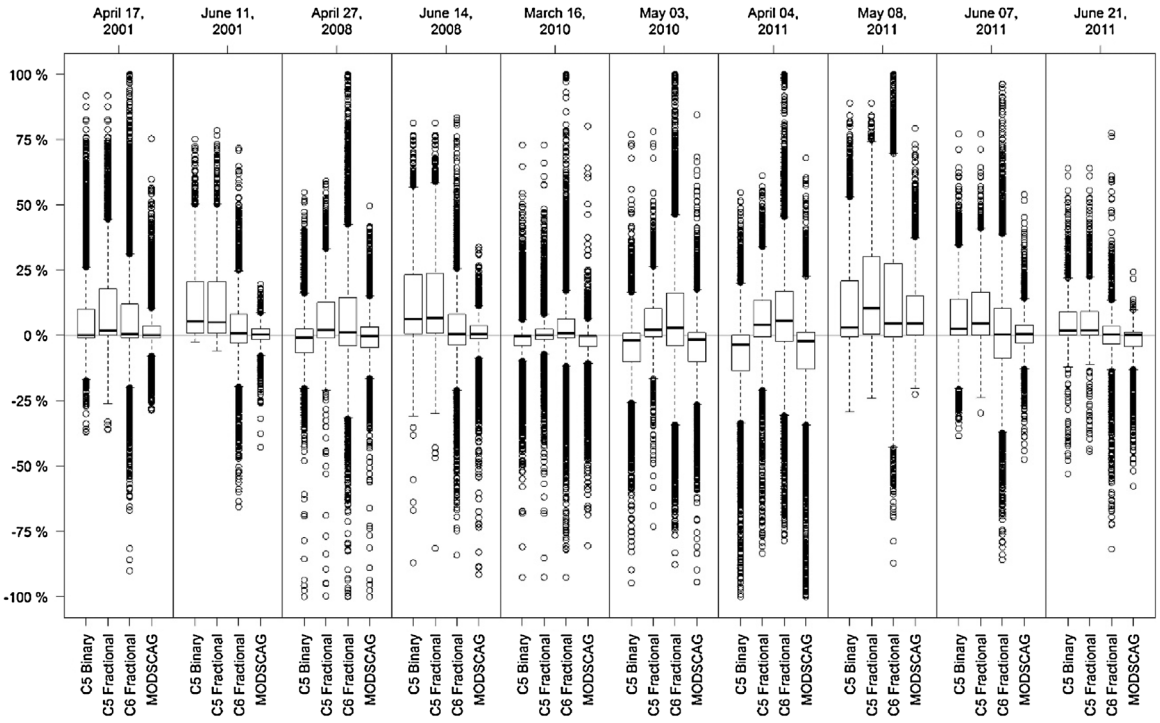

Fig. 2. Boxplots summarizing the differences between the TM binary product and the MODIS products. Positive values indicate MODIS product underestimation.

these results indicate that SCA_{BN-C5} can underestimate snow cover, even when there is early season continuous snowpack.

The locally-tuned $SCA_{F-C6-URG}$ estimates show variation across the snowmelt season. For April 2001 and 2008, the median $SCA_{F-C6-URG}$ values are closer to zero than either of the C5 products, but the data have a larger interquartile range. By comparison, for the March and May 2010 dates, and April 2011, median $SCA_{F-C6-URG}$ values are slightly further from zero than either of the C5 products. The $SCA_{F-C6-URG}$ clearly performs better than the C5 products when the snowpack becomes less continuous in the later part of the melt season (June). For all June dates, $SCA_{F-C6-URG}$ median values are less than 1% different from the SCA_{REF} median, meanwhile the C5 products can miss almost all the remaining snow, as evidenced be the position of the boxes above the 0% line in all June plots.

The seasonal variability in the results for $SCA_{F-C6-URG}$ can be explained in part because we used a single linear equation to convert from NDSI to SCA. It is likely that the NDSI:SCA relationship varies over the season in response to changes in the properties of the snowpack surface (Dozier, 1989). If this is found to be the case, a non-parametric, local regression curve fitting approach may be more appropriate (e.g., Cleveland, 1981).

The box and whisker plots demonstrate that on any individual date, a MODIS product will over-estimate and under-estimate snow cover compared to the TM product. Therefore, we have created maps for a selection of dates to illustrate the spatial distribution of the differences between MODIS-based and TM-based snow cover estimates (Fig. 3) to determine if there is an explanatory spatial component driving under- and overestimation. In Fig. 3, yellow through red shows where the TM product maps more snow cover than the MODIS product (positive difference: MODIS underestimates). Pale through dark blue hues show where the MODIS product maps more snow cover than the TM product (negative difference: MODIS overestimates). White indicates that both products agree on the area of snow cover within a 5% margin either side of 0. Grey indicates where both products agree on no snow cover. We selected three dates that show (i) different extents of snow cover and (ii) were least affected by false cloud detection at the edge of the snowpack, a well-documented source of error in C5 MOD10A1 products (Riggs et al., 2006).

On March 16, 2010 snow cover was near 100% over most of the area. SCA_{MG} shows much wider agreement with SCA_{REF} across the landscape than any of the MOD10A1 products, although there are mountain front areas at lower elevations where SCA is overestimated. SCA_{BN-C5} overestimates SCA at elevations between 2000 and 2900 m on mountain front slopes and on slopes in main headwater valley; negative differences from SCA_{REF} range from −5% to −41%. SCA_{BN-C5} underestimates SCA at the edge of the snow pack where snow cover is less continuous at the lowest elevations (positive differences ~5% to 40%). Some of these areas of underestimated SCA correspond with pixels falsely flagged as cloud cover, but the area to the northeast of the map was not strongly affected by false cloud detection. SCA_{F-C5} underestimates SCA at scattered locations at higher elevations with positive differences ranging from ~5% to 35%. Negative differences in SCA (−5% to −40%) are found at lower elevations. $SCA_{F-C6-URG}$ underestimates SCA at locations similar to SCA_{F-C5} with positive differences

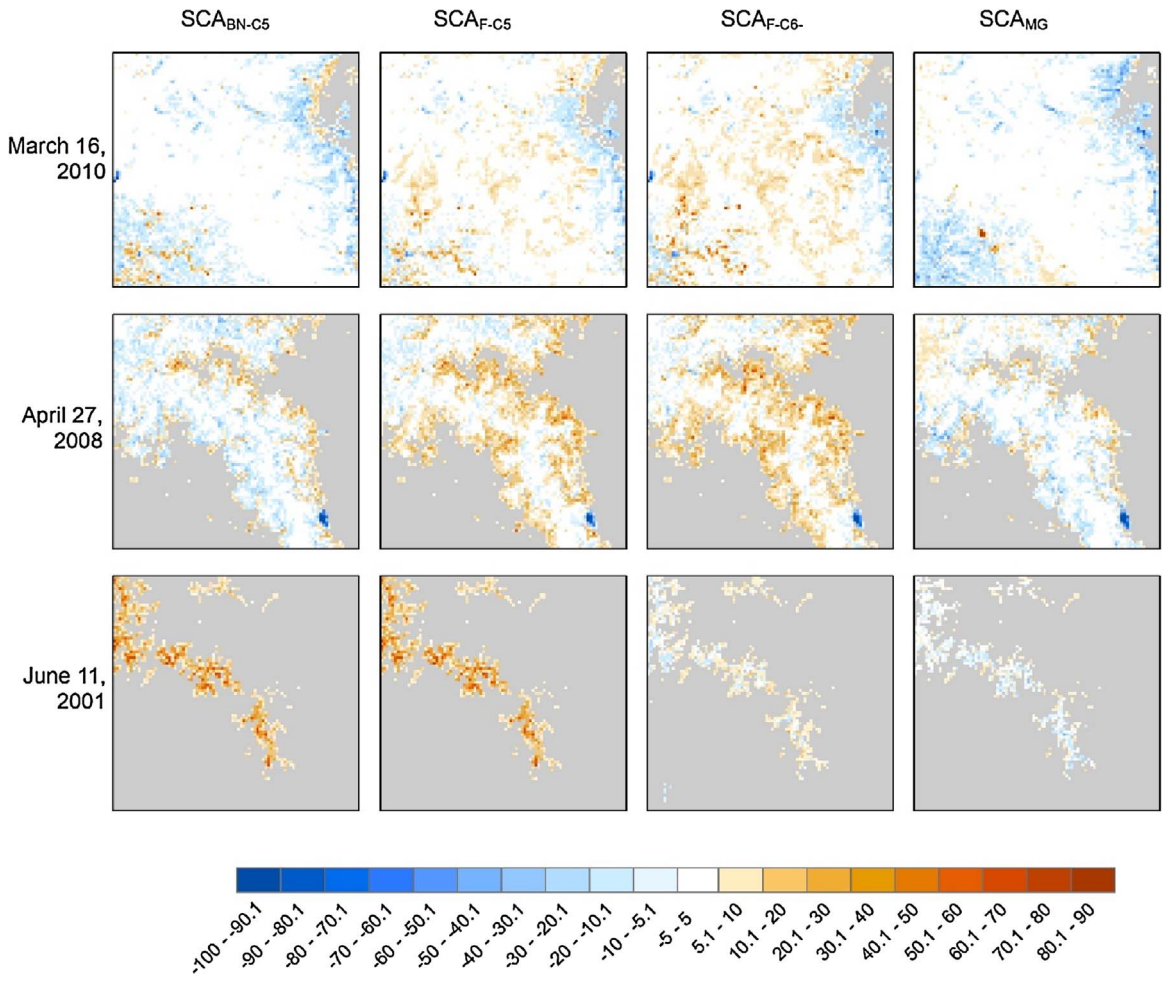

Fig. 3. Maps comparing the TM-MODIS difference in the fraction of snow cover in 1500 by 1500 m cells; blue indicates where MODIS products underestimate, red-yellow indicates where MODIS products overestimate.

in a similar range. Figs. 2 and 3 both indicate that on March 16, 2010, $SCA_{F\text{-}C6\text{-}URG}$ underestimates snow cover to a greater degree than $SCA_{F\text{-}C5}$. This is a function of the slope coefficient in the linear model.

On closer inspection both $SCA_{F\text{-}C5}$ and $SCA_{F\text{-}C6\text{-}URG}$ underestimate snow cover more frequently in forested locations than in non-forested locations. This observation would support processing the relationship between NDSI:SCA separately for forested pixels, to see if this would generate different slope and intercept coefficients in an alternate model for areas of dense vegetation.

On April 27, 2008, snow covered the San Juan Mountains, but valley bottoms and low-lying areas were snow free. Note that a small cloud was present in the TM imagery to the southeast of the study area, which means there is a patch of apparent overestimated snow cover (visible in all images). There were no cases of false cloud detection in the C5 data on this date. $SCA_{BN\text{-}C5}$ underestimates snow cover at the edge of the snowpack, where the snowpack is presumably less continuous. Both $SCA_{F\text{-}C5}$ and $SCA_{F\text{-}C6\text{-}URG}$ underestimate SCA in the same locations identified for the March 16, 2010 maps; negative differences range from ~19% to 40% over predominantly forested pixels. Locations where both $SCA_{BN\text{-}C5}$ and $SCA_{F\text{-}C5}$ overestimate SCA are more evident at higher elevations. SCA_{MG} still shows much wider agreement with SCA_{REF} than any of the C5 or C6 MOD10A1 products, but there are some locations at the edge of the snow pack where SCA_{MG} underestimates SCA. Raleigh et al. (2013) tested the MODSCAG canopy corrected SCA against a fractional TM product in subalpine meadow and forest locations and found that MODSCAG underestimated snow cover by 9–22% at meadow sites and 9–37% at forested sites.

On June 11, 2001 snow could be found at the highest elevations, mostly above the treeline. On this date, both C5 products miss almost all remaining snow cover with positive differences exceeding 40%. $SCA_{F\text{-}C6\text{-}URG}$ performs better than either C5 product with few positive differences exceeding 10%. SCA_{MG} shows better agreement with SCA_{REF} than either the C5 or C6 MOD10A1 products, but the number of cells where SCA is overestimated now exceeds the number of cells where SCA is underestimated.

3.3. Conventional depletion curves

CDCs are created by fitting non-linear regression models to the best available measurements of snow cover to give daily estimates of the proportion of each elevation zone that is covered with snow. Poor quality or cloudy data must be excluded from this analysis, especially over a small basin, because large errors in estimates of snow cover can translate to large errors in SRM simulation of streamflow. Fig. 4 shows an example of the results from 2008. In zones 1 and 2, the CDCs generated from $SCA_{F\text{-}C5}$ and $SCA_{F\text{-}C6\text{-}URG}$ trace an earlier snowmelt pattern than those generated for $SCA_{BN\text{-}C5}$ and show the most difference from those generated from SCA_{REF}. For zone 1 (2436–2926 m), the SCA_{MG} CDC aligns most closely with the SCA_{REF} CDC.

The results are a little different for zone 2 (2927–3353 m) than for zone 1; there is more variation in the April 1st estimates of snow cover between the different algorithms. CDCs modelled from SCA_{MG} and $SCA_{BN\text{-}C5}$ estimate higher snow cover than the SCA_{REF} CDC at the start of the snow melt season, while CDCs modelled from $SCA_{F\text{-}C5}$ and $SCA_{F\text{-}C6\text{-}URG}$ estimate lower snow cover. Zone 2 is the most heavily forested zone, and neither $SCA_{F\text{-}C5}$ and $SCA_{F\text{-}C6\text{-}URG}$ are explicitly corrected for sub-canopy snow cover, which might explain a proportion of the underestimation evident from the fractional products. Both SCA_{MG} and $SCA_{BN\text{-}C5}$ contain corrections for forested pixels. By May 1st, the SCA_{REF} CDC models higher snow cover than all other products. By the end of the first week of June, the SCA_{REF} and SCA_{MG} CDCs indicate there is still some snow remaining in Zone 2 (0.03), whereas the $SCA_{BN\text{-}}$, $SCA_{F\text{-}C5}$ and $SCA_{F\text{-}C6\text{-}URG}$ CDCs imply that zone 2 is snow-free.

For zone 3 (3354–4222 m), all CDCs are once again in closer agreement regarding April 1st snow cover. SCA_{MG} and $SCA_{BN\text{-}C5}$ CDCs show higher snow cover than the SCA_{REF} CDC at the beginning of the snowmelt season. The SCA_{MG} CDC moves slightly below the SCA_{REF} CDC by the third week of April, but the $SCA_{BN\text{-}C5}$ CDC continues to model a higher proportion of snow-covered area until the end of May. After this date, the amount of snow covered area modelled by the $SCA_{BN\text{-}C5}$ CDC drops sharply, and by the end of the second week of June it shows that snow is almost absent. The $SCA_{F\text{-}C6\text{-}URG}$ CDC starts the season with a lower estimate of snow cover than the other CDCs, but it performs well at indicating end-of-season SCA, giving comparable results to SCA_{MG}. For the third week of June, the SCA_{MG}, $SCA_{F\text{-}C6\text{-}URG}$ and SCA_{REF} CDCs show that Zone 3 still has between 5% and 10% snow cover.

3.4. Comparing SRM output

Table 2 summarises the results from the comparison of the hydrographs produced by SRM simulations using the different CDCs. For each year, we calibrated SRM to run with the SCA_{REF} CDCs. We did not alter the model parameters for subsequent runs that used CDCs generated from MODIS products. This means that any deviation from the runoff and volume values estimated using the base SCA_{REF} CDCs is driven by differences in the estimates of daily zonal snow-covered area. We use average runoff (Q_a), annual discharge volume and the Nash-Sutcliffe efficiency coefficient (E_f; Nash and Sutcliffe, 1970) to assess the results of the SRM simulations.

All MODIS CDCs cause SRM to underestimate Q_a and annual discharge volume, compared with both the measured streamflow data and the results from the simulations that used the SCA_{REF} CDCs (Fig. 5). Overall, CDCs modelled from the $SCA_{F\text{-}C5}$ resulted in the poorest simulations. This is because the C5 fractional product not only underestimates snow in the early snowmelt season, it misses snow cover

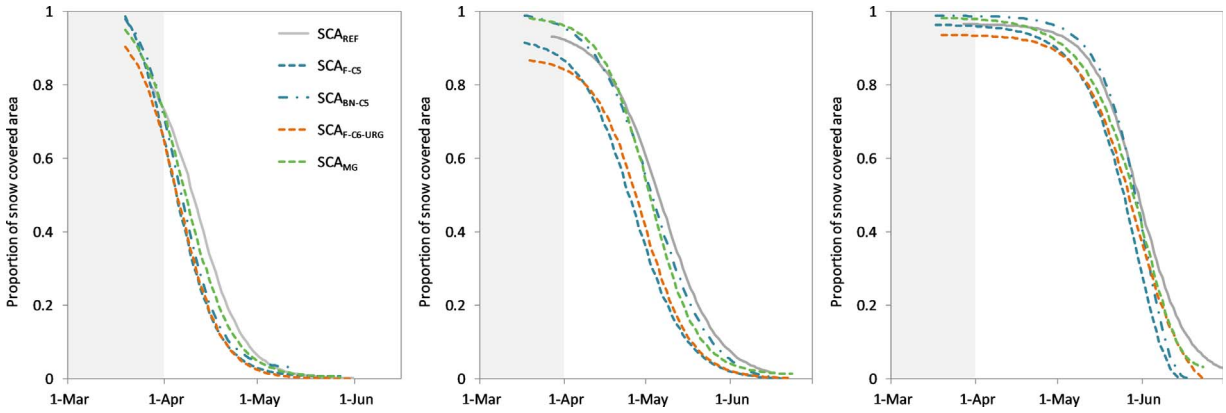

Fig. 4. Conventional depletion curves (CDCs) for 2008. Curves were created by fitting non-linear models to snow covered area against day-of-]year. April 1st is the winter end date.

Table 2
SRM simulation results.

	Volume discharge ($m^3 \times 10^6$)	Average Q ($m^3 s^{-1}$)	Volume difference ($m^3 \times 10^6$)	E_f
2001				
Stream gauge	901.35	28.58	–	–
TM [SCA_{REF}]	879.87	27.90	2.38	0.93
C5 fractional [$SCA_{F\text{-}C5}$]	597.35	18.94	33.72	0.62
C5 binary [$SCA_{BN\text{-}C5}$]	632.87	20.07	29.79	0.69
C6 [$SCA_{F\text{-}C6\text{-}URG}$]	781.36	24.77	13.31	0.91
MODSCAG [SCA_{MG}]	835.27	26.49	7.33	0.92
2008				
Stream gauge	895.56	28.32	–	–
TM [SCA_{REF}]	887.13	28.05	0.94	0.90
C5 fractional [$SCA_{F\text{-}C5}$]	688.99	21.79	23.07	0.78
C5 binary [$SCA_{BN\text{-}C5}$]	809.40	25.60	9.62	0.85
C6 [$SCA_{F\text{-}C6\text{-}URG}$]	743.43	23.51	16.99	0.85
MODSCAG [SCA_{MG}]	803.22	25.40	10.31	0.89
2010				
Stream gauge	650.45	20.63	–	–
TM [SCA_{REF}]	636.03	20.17	2.22	0.83
C5 fractional [$SCA_{F\text{-}C5}$]	509.16	16.15	21.72	0.63
C5 binary [$SCA_{BN\text{-}C5}$]	631.88	20.04	2.85	0.70
C6 [$SCA_{F\text{-}C6\text{-}URG}$]	574.90	18.23	11.62	0.73
MODSCAG [SCA_{MG}]	602.67	19.11	7.35	0.73
2011				
Stream gauge	619.90	19.66	–	–
TM [SCA_{REF}]	613.65	19.46	1.01	0.95
C5 fractional [$SCA_{F\text{-}C5}$]	455.49	14.44	26.52	0.64
C5 binary [$SCA_{BN\text{-}C5}$]	495.60	15.72	20.05	0.72
C6 [$SCA_{F\text{-}C6\text{-}URG}$]	517.89	16.42	16.46	0.83
MODSCAG [SCA_{MG}]	551.60	17.49	11.02	0.88

completely at the end of the snowmelt season. CDCs modelled from SCA_{MG} performed well, leading to relatively small underestimates (~7–11%) in annual discharge volume compared to the measured discharge volume. This result is expected given the close agreement between SCA_{MG} and SCA_{REF}.

The simulations that used the $SCA_{F\text{-}C6\text{-}URG}$ CDCs yielded better results in 2001 and 2011 than the $SCA_{BN\text{-}C5}$ simulations, with higher E_f values and lower volume differences. Even in 2008 and 2010, where the $SCA_{BN\text{-}C5}$ simulations yielded lower volume differences than the $SCA_{F\text{-}C6\text{-}URG}$ simulations, the resulting $SCA_{F\text{-}C6\text{-}URG}$, E_f values were equivalent (2008) or higher than (2010) those resulting from the $_{SCA_{BN\text{-}C5}}$5 simulations. The reason for this is twofold. Firstly, as intended, the $SCA_{F\text{-}C6\text{-}URG}$ is more sensitive to end of season snow cover than the C5 products, so the $SCA_{F\text{-}C6\text{-}URG}$ simulation continues to receive input from snow in late May and June, whereas for the same dates C5 inputs determine snow cover is absent and therefore the C5 simulations no longer add snowmelt to the stream discharge. By itself, this may not be sufficient to cause a large difference in Q_a and annual discharge volume. However, when the difference in estimates of end-of-season snow covered area coincides with a relatively high C_s coefficient (the proportion of snowmelt runoff contributing to runoff), then the difference between the C5 and C6 simulation results will be amplified. Secondly, for the 2008 and 2010 simulations, the hydrographs produced by the $SCA_{BN\text{-}C5}$ simulations show that simulated Q first exceeds, then drops below measured Q (Fig. 5). In these cases, early season overestimation of SCA and snow inputs to runoff compensates for late season underestimation with respect to the overall volume difference. Even though the simulation results for annual discharge volume and Q_a are somewhat closer to the measured values than those for the $SCA_{F\text{-}C6\text{-}URG}$, this result does not necessarily support recommendation of the C5 Binary product because the balance between overestimation and underestimation merely represents the offset of one systematic error against another.

We note that for the 2010 water year, all simulations performed relatively poorly compared to the other years. The accuracy of the SCA_{REF} maps is slightly lower for 2010 than for other years (Table 1) so this is likely to have affected SRM calibration. It is also possible that the relationship between air temperature and snow melt was complicated by other factors in this relatively dry year.

4. Conclusion

The selection of snow cover product is important when using a TI model such as SRM. During calibration, snowmelt function model parameters (α, c_s, c_r) can be inadvertently altered to account for insufficiencies in SCA. This impacts model results and propagates error into climate change simulations. While Landsat sensors provide optimal spatial resolution for mapping patterns of snowmelt in smaller basins, the temporal resolution of acquisitions provides fewer images to capture depletion patterns over the snowmelt season. Terra MODIS has a higher temporal resolution than Landsat sensors, but the spatial resolution of the data is limiting over areas of patchy, discontinuous snow. Of the MODIS products tested here, canopy-corrected SCA from MODSCAG performed more consistently than MOD10A1 products yielding SCA estimates that were close to those derived from Landsat TM. When used as SCA input to SRM, CDCs modelled from MODSCAG resulted in higher E_f values and lower differences from measured discharge volume. However, we see potential in using the global C6 NDSI snow cover product to generate a locally-tuned snow product based on developing empirical relations between NDSI and SCA for different snow conditions and land covers. This may be accomplished using the empirical approach described in Salomonsson and Appel (2004). Alternatively, users can apply the binary algorithm used in Collection 5, but should test the NDSI thresholds used within the algorithm to ensure they are appropriate for their study area (Riggs et al., 2016). The results for the canopy-corrected MODSCAG SCA support the application of some type of correction for snow present under the forest canopy but not visible to the sensor. Future work following on from this paper will explore potential empirical models for relating the C6 NDSI to snow cover over our southern Rocky Mountain study basins.

There will be error associated with any snow product, whether it is empirical or physically-based and acquired as a product or produced "in-house". There may be some advantage in using an ensemble of products, especially when the temporal frequency of data acquisition is low. For example; SCA estimates from MODIS snow cover data sets can be combined with estimates with from finer spatial resolution imagery. Our last words here are to advise that whichever products are selected to produce input for hydrological modelling, that all sources of error are recognized and understood so that error propagation and subsequent model over fitting are minimized.

Acknowledgements

The authors thank Jaroslav Martinec for his help in parameterizing SRM for the Del Norte basin and others in the Upper Rio Grande Basin. We also thank the anonymous reviewers and editor whose comments and encouragement helped us to improve this paper. This study was funded by the National Science Foundation grant #814449: New Mexico EPSCoR.

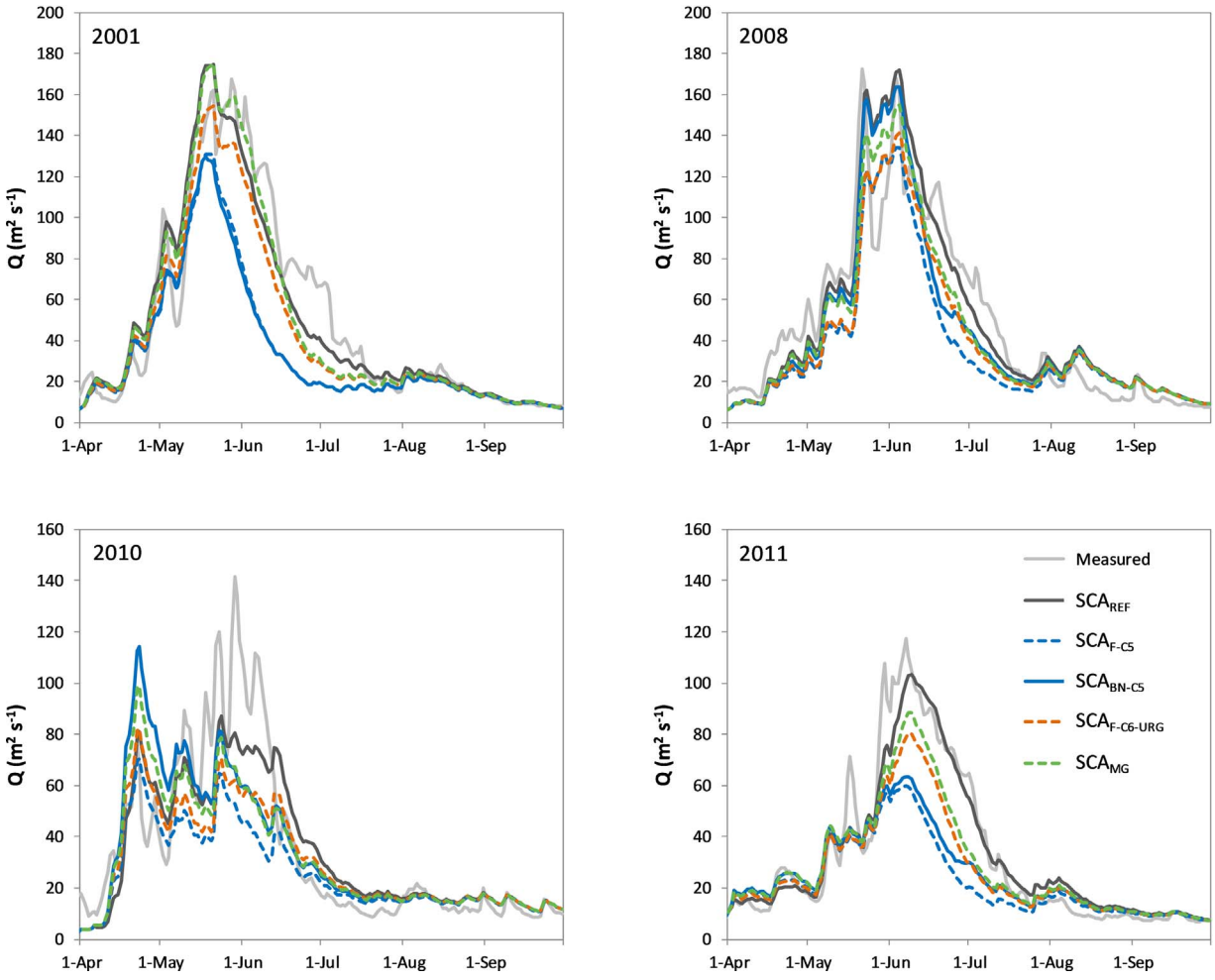

Fig. 5. Comparison of the SRM simulations.

References

Anderson, E.A., 1976. A Point Energy and Mass Balance Model of a Snow Cover, NOAA Technical Report NWS-19. 150 pp.

Andreadis, K.M., Lettenmaier, D.P., 2006. Assimilating remotely sensed snow observations into a macroscale hydrology model. Adv. Water Resour. 29, 872–886. http://dx.doi.org/10.1016/j.advwatres.2005.08.004.

Cleveland, W.S., 1981. LOWESS: A program for smoothing scatterplots by robust locally weighted regression. Am. Stat. 35, 54. http://dx.doi.org/10.2307/2683591.

Day, C.A., 2009. Modelling impacts of climate change on snowmelt runoff generation and streamflow across western US mountain basins: a review of techniques and applications for water resource management. Prog. Phys. Geogr. 33, 1–20. http://dx.doi.org/10.1177/0309133309343131.

Dozier, J., 1989. Spectral signature of alpine snow cover from the landsat thematic mapper. Remote Sens. Environ. 28, 9–22.

Earth Observing System Data and Information System (EOSDIS), 2009, Earth Observing System ClearingHouse (ECHO)/Reverb Version 10. X [online application]. Greenbelt, MD: EOSDIS, Goddard Space Flight Center (GSFC) National Aeronautics and Space Administration (NASA). URL: https://reverb.echo.nasa.gov/reverb (Accessed 19 Januray 2017).

ESRI, 2015. ArcGIS Desktop: Release 10.2. Environmental Systems Research Institute, Redlands, CA.

ESRI, 2016. World Imagery Map Service. http://services.arcgisonline.com/ArcGIS/rest/services/World_Imagery/MapServe.

Elias, E., Rango, A., Steele, C.M., Mejia, J.F., Smith, R., 2015. Assessing climate change impacts on water availability of snowmelt-dominated basins of the Upper Rio Grande basin. J. Hydrol.: Reg. Stud. 3, 525–546. http://dx.doi.org/10.1016/j.ejrh.2015.04.004.

Garen, D.C., Marks, D., 2005. Spatially distributed energy balance snowmelt modelling in a mountainous river basin: estimation of meteorological inputs and verification of model results. J. Hydrol. 315, 126–153. http://dx.doi.org/10.1016/j.jhydrol.2005.03.026.

Georgievsky, M.V., 2009. Application of the snowmelt runoff model in the Kuban river basin using MODIS satellite images. Environ. Res. Lett. 4, 45017. http://dx.doi.org/10.1088/1748-9326/4/4/045017.

Hall, D.K., Riggs, G.A., 2007. Accuracy assessment of the MODIS snow products. Hydrol. Processes 21, 1534–1547. http://dx.doi.org/10.1002/hyp.6715.

Hall, D.K., Riggs, G.A., 2016. MODIS/Terra Snow Cover Daily L3 Global 500 m Grid, Version 6. [NDSI Snow Cover (h09v05)]. NASA National Snow and Ice Data Center Distributed Active Archive Center, Boulder, Colorado USA. http://dx.doi.org/10.5067/MODIS/MOD10A1.006.. Data available from: https://reverb.echo.nasa.gov/reverb/ (Accessed 19 July 2017).

Hall, D.K., Riggs, G.A., Salomonson, V.V., 1995. Development of methods for mapping global snow cover using moderate resolution imaging spectroradiometer data. Remote Sens. Environ. 54, 127–140. http://dx.doi.org/10.1016/0034-4257(95)00137-P.

Hall, D.K., Salomonson, V.V., Riggs, G.A., 2006. MODIS/Terra Snow Cover Daily L3 Global 500 M Grid, Version 5, [Binary, Fractional]. NASA National Snow and Ice Data Center Distributed Active Archive Center, Boulder, Colorado, USA.

Hock, R., 2003. Temperature index melt modelling in mountain areas. J. Hydrol. 282, 104–115. http://dx.doi.org/10.1016/S0022-1694(03)00257-9.

Homan, J.W., Luce, C.H., McNamara, J.P., Glenn, N.F., 2011. Improvement of distributed snowmelt energy balance modeling with MODIS-based NDSI-derived fractional snow-covered area data. Hydrol. Processes 25, 650–660. http://dx.doi.org/10.1002/hyp.7857.

Immerzeel, W.W., Droogers, P., de Jong, S.M., Bierkens, M.F.P., 2009. Large-scale monitoring of snow cover and runoff simulation in Himalayan river basins using remote sensing. Remote Sens. Environ. 113, 40–49. http://dx.doi.org/10.1016/j.rse.2008.08.010.

Klein, A.G., Hall, D.K., Riggs, G.A., 1998. Improving snow cover mapping in forests through the use of a canopy reflectance model. Hydrol. Processes 12, 1723–1744. http://dx.doi.org/10.1002/(SICI)1099-1085(199808/09)12:10/11<1723:AID-HYP691>3.0.CO;2-2.

Kumar, M., Marks, D., Dozier, J., Reba, M., Winstral, A., 2013. Evaluation of distributed hydrologic impacts of temperature-index and energy-based snow models. Adv. Water Resour. 56, 77–89. http://dx.doi.org/10.1016/j.advwatres.2013.03.006.

Lee, S., Klein, A., Over, T.M., 2005. A comparison of MODIS and NOHRSC snow-cover products for simulating streamflow using the snowmelt runoff model. Hydrol. Processes 19, 2951–2972. http://dx.doi.org/10.1002/hyp.5810.

Li, X., Williams, M.W., 2008. Snowmelt runoff modelling in an arid mountain watershed, Tarim basin, China. Hydrol. Processes 22, 3931–3940. http://dx.doi.org/10.1002/hyp.7098.

Marks, D., Domingo, J., Susong, D., Link, T., Garen, D., 1999. A spatially distributed

energy balance snowmelt model for application in mountain basins. Hydrol. Processes 13, 1935–1959. http://dx.doi.org/10.1002/(SICI)1099-1085(199909)13:12/13<1935:AID-HYP868>3.0.CO;2-C.

Martinec, J., Rango, A., Major, E., 1983. The Snowmelt-Runoff Model (SRM) User's Manual. NASA Reference Publication 1100, Washington D.C 118 pp.

Martinec, J., Rango, A., Roberts, R., 2008. Snowmelt Runoff Model (SRM) User's Manual. College of Agriculture and Home Economics, New Mexico State University, Las Cruces, NM, USA 178 pp.

NOAA, 2016. National Climatic Data Center, Cooperative Observer Network. http://www.ncdc.noaa.gov/data-access/land-based-station-data.

NRCS, 2016. Snow Telemetry (SNOTEL) and Snow Course Data and Products. http://www.wcc.nrcs.usda.gov/snow/.

Nash, J.E., Sutcliffe, J.V., 1970. River flow forecasting through conceptual models. Part 1: a discussion of principles. J. Hydrol. 10, 282–290. http://dx.doi.org/10.1016/0022-1694(70)90255-6.

Ohmura, A., 2001. Physical basis for the temperature-based melt-index method. J. Appl. Meteorol. Climatol. 40, 753–761. http://dx.doi.org/10.1175/1520-0450(2001)040<0753:PBFTTB>2.0.CO;2.

Painter, T.H., Rittger, K., McKenzie, C., Slaughter, P., Davis, R.E., Dozier, J., 2009. Retrieval of subpixel snow covered area, grain size, and albedo from MODIS. Remote Sens. Environ. 113, 868–879. http://dx.doi.org/10.1016/j.rse.2009.01.001. Data Accessed online on 21 May 2016.

Panday, P.K., Williams, C.A., Frey, K.E., Brown, M.E., 2013. Application and evaluation of a snowmelt runoff model in the Tamor River basin, Eastern Himalaya using a Markov Chain Monte Carlo (MCMC) data assimilation approach. Hydrol. Processes 5337–5353. http://dx.doi.org/10.1002/hyp.10005.

Pederson, G.T., Gray, S.T., Woodhouse, C.A., Betancourt, J.L., Fagre, D.B., Littell, J.S., Watson, E., Luckman, B.H., Graumlich, L.J., 2011. The unusual nature of recent snowpack declines in the North American Cordillera. Science 333, 332–335. http://dx.doi.org/10.1126/science.1201570.

Raleigh, M.S., Rittger, K., Moore, C.E., Henn, B., Lutz, J.A., Lundquist, J.D., 2013. Ground-based testing of MODIS fractional snow cover in subalpine meadows and forests of the Sierra Nevada. Remote Sens. Environ. 128, 44–57. http://dx.doi.org/10.1016/j.rse.2012.09.016.

Rango, A., Martinec, J., 1979. Application of a snowmelt runoff model using landsat data. Nordic Hydrol. 10, 225–238.

Riggs, G.A., Hall, D.K., Salomonson, V.V., 1994. A snow index for the landsat thematic mapper and moderate resolution imaging spectroradiometer. In: Proceedings of the International Geoscience and Remote Sensing Symposium, IGARSS '94. Pasadena, California, IEEE. pp. 1942–1944. http://dx.doi.org/10.1109/IGARSS.1994.399618.

Riggs, G.A., Hall, D.K., Salomonson, V.V., 2006. MODIS Snow Products User Guide to Collection 5. Available online at. http://modis-snow-ice.gsfc.nasa.gov/uploads/sug_c5.pdf.

Riggs, G.A., Hall, D.K., Román, M.O., 2016. MODIS Snow Products Collection 6 User Guide. Available online at. http://modis-snow-ice.gsfc.nasa.gov/uploads/C6_MODIS_Snow_User_Guide.pdf.

Rittger, K., Painter, T.H., Dozier, J., 2013. Assessment of methods for mapping snow cover from MODIS. Adv. Water Resour. 51, 367–380. http://dx.doi.org/10.1016/j.advwatres.2012.03.002.

Salomonsson, V.V., Appel, I., 2004. Estimating fractional snow cover from MODIS using the normalized difference snow index. Remote Sens. Environ. 89, 351–360. http://dx.doi.org/10.1016/j.rse.2003.10.016.

Shreve, C.M., Okin, G.S., Painter, T.H., 2009. Indices for estimating fractional snow cover in the western Tibetan Plateau. J. Glaciol. 55, 737–745.

Stewart, I.T., Cayan, D.R., Dettinger, M.D., 2004. Changes in snowmelt runoff timing in western north america under a 'business as usual' climate change scenario. Clim. Change 62, 217–232. http://dx.doi.org/10.1023/B:CLIM.0000013702.22656.e8.

Tekeli, A.E., Akyürek, Z., Şorman, A.A., Şensoy, A., Sorman, A.U., 2005. Using MODIS snow cover maps in modelling snowmelt runoff process in the eastern part of Turkey. Remote Sens. Environ. 97, 216–230. http://dx.doi.org/10.1016/j.rse.2005.03.013.

Tukey, J.W., 1977. Exploratory Data Analysis. Addison-Wesley, Reading, MA 668 p.

USGS, 2016a. Climate Data Record (CDR) Landsat Surface Reflectance High Level Data Products. http://earthexplorer.usgs.gov/.

USGS, 2016b. National Water Information System. http://waterdata.usgs.gov/nwis.

Xin, Q., Woodcock, C.E., Liu, J., Tan, B., Melloh, R.A., 2012. View angle effects on MODIS snow mapping in forests. Remote Sens. Environ. 118, 50–59. http://dx.doi.org/10.1016/j.rse.2011.10.029.